Earth and Planetary Science Letters, 79 (1986) 217–234
Elsevier Science Publishers B.V., Amsterdam – Printed in The Netherlands

[1]

The abundance and relative volatility of refractory trace elements in Allende Ca,Al-rich inclusions: implications for chemical and physical processes in the solar nebula

Alan S. Kornacki [1,*] and Bruce Fegley, Jr. [2,**]

[1] *Shell Western E & P, Inc., P.O. Box 831, Houston, TX 77001 (U.S.A.)*
[2] *Department of Earth, Atmospheric, and Planetary Sciences, Massachusetts Institute of Technology, Cambridge, MA 02139 (U.S.A.)*

Received October 8, 1985; revised version accepted May 27, 1986

We have determined the relative volatility of lithophile refractory trace elements (LRTE) in the solar nebula by first calculating 50% condensation temperatures for 26 LRTE oxides (assuming ideal solid solution in perovskite and, where appropriate, in hibonite and melilite). The measured abundances of 25 LRTE and six siderophile refractory trace elements in 97 Group I, II, III, and V Allende Ca,Al-rich inclusions (CAI's) and in ultra-refractory inclusions then are used to empirically modify LRTE and refractory siderophile volatility sequences that are based on condensation temperatures alone. Sc is significantly less depleted in Group II Allende CAI's than are other LRTE (e.g., Zr; Hf; Y) that also have very high oxide condensation temperatures; Ba, Sr, and Eu (three moderately volatile LRTE) are significantly more enriched in Ca-rich Group II and Group III Allende CAI's than they are in spinel-rich varieties of these inclusions. We explain these observations and several others by invoking dust fractionations, and crystal-chemical and diffusion effects during the formation of Allende CAI's that overprinted volatility based on solid/gas reactions alone. For example, we show that hibonite probably was not the carrier of the super-refractory lithophile component that is missing from Group II Allende inclusions. Anomalous Hf depletions (relative to Zr and Y) that are common in Group I, III, and V Allende CAI's can be partly explained if Anders and Ebihara [38] overestimated the cosmic abundance of Hf by approximately 10%.

1. Introduction

Ca,Al-rich inclusions (CAI's) in the Allende CV3 chondrite are highly enriched (relative to chondritic abundances) in the lithophile and siderophile refractory trace elements [1]. These enrichments are evidence that the chemistry of CAI's was established at high temperatures in the solar nebula [2,3]. The refractory trace-element abundance patterns in Allende CAI's also provide valuable information about chemical and physical processes in the regions of the solar nebula where the inclusions formed. For example, it has been suggested that the highly-fractionated Group II REE patterns in some CAI's are due to interrupted, multistage condensation processes in the solar nebula [4], and that Mo and W depletions indicate that the refractory siderophiles in CAI's commonly were processed at high temperatures in relatively oxidized regions of the solar nebula [5]. Additional, albeit incompletely understood, information about nebular processes is provided by the other REE patterns in CAI's [6].

In this paper, we first determine average refractory trace-element abundances in approximately 100 Allende inclusions. We then develop a relative volatility sequence for 26 lithophile refractory trace elements (LRTE) that is based on 50% condensation temperatures that we calculate, assuming ideal oxide solid solution in perovskite and (where appropriate) hibonite and melilite. We subsequently use the trace-element abundance patterns in Allende CAI's and ultra-refractory inclusions to empirically modify our calculated LRTE volatility sequence. Finally, we discuss the importance of crystal-chemical effects, diffusion constraints, and grain transport for the origin of the trace-element chemistry of Allende CAI's (which have important implications for chemical and physical processes in the solar nebula).

* Present address: Shell Development Company, Bellaire Research Center, P.O. Box 481, Houston, TX 77001, U.S.A.
** Also: Max-Planck-Institut für Chemie (Otto-Hahn-Institut), Saarstrasse 23, D-6500 Mainz, F.R.G.

0012-821X/86/$03.50

2. Methods

2.1. Refractory trace-element abundances

Trace-element abundances were compiled from all available sources [1,6–18] for 51 Group I and V CAI's, 12 Group III CAI's, and 34 Group II CAI's. Group I and V CAI's have relatively flat REE patterns, Group III CAI's have flat REE patterns except for negative Eu and Yb anomalies, and Group II CAI's are relatively depleted in Eu and the heavy REE (excluding Tm) [16]. We further subdivided Group II and Group III CAI's into two broad types: Ca-rich and Ca-poor. The Ca-rich inclusions comprise the melilite-rich Type A, fassaite-rich Type B, and plagioclase-rich Type C CAI's [3,18]; they typically are relatively coarse-grained. The Ca-poor inclusions include spinel-rich Type F aggregates [18], and Type 2 or Type 3B inclusions [19]; they typically are relatively fine-grained.

Sources of potential error in our compilation of published abundance data are the errors due to sampling heterogeneous CAI's, and to systematic differences in the analytical techniques and standards used by different laboratories. We evaluated the magnitude of these errors by comparing analyses of the same inclusion reported by different laboratories. Tanaka and Masuda [7] and Mason and Taylor [16] each measured the abundances of nine REE and Ba in the Group III CAI 3529-0: their results differed by $< 20\%$ for all elements except Sm (21.4%). Mason and Martin [6] and Conard [10] each measured the abundances of 13 REE, Hf, and Ba in the Group I CAI 3898: their results differed by $\leqslant 20\%$ for all elements except Er (22.2%), Ho (27.5%), and Ba (29.4%). This comparison of inter-laboratory analyses of the only Allende inclusions included in our compilation for which data from more than one laboratory are available suggests that systematic errors between laboratories typically are not very large.

Another source of error is the relative precision of the trace-element abundance measurements. For example, Wänke et al. [1] estimated that the $\pm 1\sigma$ standard deviations in their abundance measurements were 20% for Nb, Ce, Gd, and Ta; 15% for Y; and 10% or less for 15 other LRTE and six refractory siderophiles in a Group I Allende CAI. In this paper, the magnitudes of important chemical patterns, anomalies, and features we discuss in all cases are greater than the 1σ standard deviations in relative analytical precisions for the trace element(s) of interest.

We encountered a problem using literature data to determine the absolute abundances of refractory siderophiles in spinel-rich Group II Allende inclusions. Mason and Taylor [16] and H. Palme (unpublished) each measured the abundance of two or more refractory siderophiles in five spinel-rich Group II inclusions. In four of these CAI's, Ir concentrations range from 0.34 to 0.87 ppm (i.e., ~ 0.7–$1.8\times$ chondritic levels), and the other refractory siderophiles analyzed typically occur at ~ 0.2–$2.0\times$ chondritic levels. In sharp contrast, Ir occurs at a concentration of $\leqslant 0.30$ ppm in all 11 spinel-rich Group II Allende inclusions analyzed by Conard [10], Grossman and Ganapathy [12], and Nagasawa et al. [13]. Unfortunately, none of the other refractory siderophiles were analyzed in the 11 Ir-poor CAI's, but we consider it very likely that all refractory siderophiles are significantly more depleted in them than in the five inclusions analyzed in more detail by Mason and Taylor [16] and H. Palme (unpublished). But because we were primarily interested in comparing enrichment trends among *all* refractory siderophiles in the various types of Allende inclusions, we used only data from the five spinel-rich Group II inclusions in which two or (generally) more refractory siderophiles were analyzed. Although the relatively high concentrations of refractory siderophiles in the Group II inclusions we used could simply be due to contamination by metal-bearing meteorite matrix (H. Palme, personal communication, 1984), we discuss why we do not support this interpretation in section 5.1.

2.2. Lithophile refractory trace element condensation calculations

The relative volatilities of 26 LRTE were calculated for a large range of temperatures and pressures by computing the 50% condensation temperatures for ideal oxide solid solution in perovskite, which was adopted as a baseline model for several reasons: (1) perovskite probably is an important host for many LRTE in Allende CAI's; (2) this model allows easy comparison of the 50% condensation temperatures of the LRTE, refractory siderophiles, and major elements; and (3)

ideal solid solution provides a convenient starting point for investigating crystal-chemical effects on the relative volatility of LRTE. We also calculated the 50% condensation temperatures for selected LRTE in hibonite and melilite (see sections 3 and 5.2). Furthermore, we studied the effects of variable (assumed) activity coefficients on the condensation of selected LRTE in perovskite, since activity coefficients are not known for the relevant LRTE solid solutions in perovskite or other potential CAI host phases. Our condensation calculations should be very useful for evaluating models of the origin of Group II inclusions, some of which require the removal or isolation of refractory dust grains from nebular gas at very specific temperatures [20,21].

Thermodynamic data sources. Approximately 150 gaseous and solid compounds of 26 LRTE were included in the calculations. All of the compounds considered and the thermodynamic data sources used are listed in Table 1. The necessary equilibrium constants used in the calculations either were taken directly from standard compilations or were calculated by the Third Law method (described in the JANAF Tables). Equilibrium constants for REE monoxide gases were calculated using Gibbs energy functions from E. Murad (personal communication, 1984) and enthalpies in Murad and Hildenbrand [22], who showed that their revised REE monoxide gas thermodynamic data are in better accord than older data with changes in the $4f^n6s^2 \rightarrow 4f^{n-1}5d6s^2$ electronic promotion energies in the gaseous metal atoms. We fit the equilibrium constants for most compounds in Table 1 to linear equations of the form $\log_{10} K = A/T + B$, where K is the equilibrium constant for formation from the elements in their respective reference states. However, we used quadratic or cubic equations for $\log_{10} K$ when necessary. We also made proper allowances for changes in the elemental reference states when fitting these equations.

Method of calculation. The solid solution of LRTE oxides in perovskite, hibonite, and melilite was

TABLE 1

Thermodynamic data sources for compounds included in the calculations

Data source	Compounds
	Gases
JANAF [5] [a]	Zr, ZrO, ZrO_2, Ta, TaO, TaO_2, V, VO, VO_2, Nb, NbO, NbO_2, Ba, BaO, BaOH, $Ba(OH)_2$, BaS, BaCl, $BaCl_2$, BaF, BaF_2, Sr, SrO, SrOH, $Sr(OH)_2$, SrS, SrCl, $SrCl_2$, SrF, SrF_2
Hultgren et al. [5] [a]	La, Ce, Pr, Nd, Sm, Eu, Gd, Tb, Dy, Ho, Er, Tm, Yb, Lu
Murad (unpubl.), Murad and Hildenbrand [22]	LaO, PrO, NdO, SmO, EuO, GdO, TbO, DyO, HoO, ErO, TmO, YbO, LuO
Mignanelli et al. [23]	CeO, CeO_2
Kordis and Gingerich [24]	Ce_2O_2, Gd_2O_2, Gd_2O, Tb_2O_2, Tb_2O, Ho_2O_2, Ho_2O, Eu_2O_2, Eu_2O, Lu_2O
Glushko et al. [25]	BaH, SrH, La_2O, La_2O_2, Pu, PuO, PuO_2, Sc, ScO, Sc_2O, Sc_2O_2, Y, YO, Y_2O, Y_2O_2, Hf, HfO, HfO_2
Ackermann and Chandrasekharaiah [26]	U, UO, UO_2, UO_3, Th, ThO, ThO_2
	Solids
Robie et al. [5] [a]	La_2O_3, Pr_2O_3, Nd_2O_3, Sm_2O_3, EuO, Eu_2O_3, Gd_2O_3, Tb_2O_3, Dy_2O_3, Ho_2O_3, Er_2O_3, Lu_2O_3
Gschneidner et al. [27]	CeO_2, Ce_2O_3, Eu_3O_4, Tm_2O_3, Yb_2O_3
JANAF [5] [a]	NbO, NbO_2, Nb_2O_5, VO, V_2O_3, V_2O_4, V_2O_5, Ta_2O_5, BaO, SrO
Ackermann and Chandrasekharaiah [26]	UO, UO_2, U_2O_3, ThO_2
Glushko et al. [25]	UO_3, U_3O_8, U_4O_9, PuO_2, Pu_2O_3, Y_2O_3, HfO_2
Pankratz [28]	PuO, Sc_2O_3, ZrO_2
Kelley [5] [a]	$SrTiO_3$, Sr_2TiO_4, $BaTiO_3$, Ba_2TiO_4
Parker et al. [29]	$CaZrO_3$, $SrTiO_3$, Sr_2TiO_4, $BaTiO_3$, Ba_2TiO_4, $BaZrO_3$, $SrZrO_3$
Levitskii et al. [30]	$SrZrO_3$
Odoz and Hilpert [31]	$BaZrO_3$

[a] Original reference can be found in Fegley and Palme [5].

calculated using the multicomponent gas-solid chemical equilibrium program METKON [5] expanded by B. Fegley, Jr., H. Kruse, and H. Palme to include LRTE condensation. The calculations, which were performed in a way analogous to that first described by Boynton [4], can be illustrated with an example for Sm.

The vapor-solid equilibrium for Sm can be written as:

$$SmO(g) + \tfrac{1}{2}H_2O(g) = SmO_{1.5}(s) + \tfrac{1}{2}H_2(g) \quad (1)$$

and the partial pressure of SmO(g) in equilibrium with a solid phase containing $SmO_{1.5}$ is given by:

$$P_{SmO}(g) = \left[a(SmO_{1.5})/K_1\right]\left[P_{H_2}/P_{H_2O}\right]^{1/2} \quad (2)$$

where $a(SmO_{1.5})$ is the activity of $SmO_{1.5}$ in the solid and K_1 is the equilibrium constant for equation (1). The partial pressure of SmO(g) in the nebula is given by:

$$P_{SmO}(neb) = \left[A(Sm)/A(H_2 + He)\right] \times \beta_{SmO}(1 - \alpha_{Sm})P_T \quad (3)$$

where $A(Sm)$ and $A(H_2 + He)$ are the cosmic abundances of Sm and $H_2 + He$, β_{SmO} is the fraction of Sm in the gas present as SmO, α_{Sm} is the fraction of total Sm condensed in the solid phase, and P_T is the total nebular pressure. At equilibrium:

$$P_{SmO}(g) = P_{SmO}(neb) \quad (4)$$

and the fraction of Sm condensed is given by:

$$\alpha_{Sm} = 1 - \frac{a(SmO_{1.5})}{K_1}\left(\frac{P_{H_2}}{P_{H_2O}}\right)^{1/2}\frac{A(H_2 + He)}{A(Sm)\beta_{SmO}P_T} \quad (5)$$

Assuming the perovskite is the host phase for Sm, the activity of $SmO_{1.5}$ in perovskite is given by:

$$a(SmO_{1.5}) = \gamma(SmO_{1.5})\,X(SmO_{1.5}) \quad (6)$$

where:

$$X(SmO_{1.5}) = \frac{\alpha_{Sm}A(Sm)f_{Sm}}{\alpha_{Ti}A(Ti) + \sum_i \alpha_i A(i)} \quad (7)$$

$\alpha_{Ti}A(Ti)$ is the amount of perovskite condensed and f_{Sm} is the fraction of Sm in perovskite present as $SmO_{1.5}$. (If no other solid Sm species are considered, $f_{Sm} = 1$.) The summation in the denominator of equation (7) accounts for the amounts of all other LRTE dissolved in perovskite, but this term can be neglected because of the much smaller abundances of the LRTE relative to the abundance of Ti. Combining equations (5) and (7) yields an expression for α_{Sm}:

$$\alpha_{Sm} = \left[1 + \frac{A(H_2 + He)}{\alpha_{Ti}A(Ti)}\left(\frac{P_{H_2}}{P_{H_2O}}\right)^{1/2} \times \frac{\gamma(SmO_{1.5})}{K_1}\frac{f_{Sm}}{\beta_{SmO}}\frac{1}{P_T}\right]^{-1} \quad (8)$$

From equation (8) it is apparent that the fraction of Sm (or any other LRTE) condensed is independent of its abundance. Similar equations were written for the other LRTE, taking into account the appropriate changes in stoichiometry for condensation of solid monoxides, dioxides, pentoxides, and so forth. One such equation is required for every LRTE oxide in perovskite.

Before solving these equations, we calculated several input parameters. The fraction of Ti condensed as perovskite (α_{Ti}) was calculated from major-element condensation calculations [32]; the H_2/H_2O ratio also was obtained from those calculations (or can be varied appropriately to study condensation at oxygen fugacities other than the canonical solar nebular value). Solid oxide activity coefficients (γ's) were set equal to 1 (unless stated otherwise). The equilibrium constants equivalent to K_1 were calculated from the thermodynamic data in Table 1 and JANAF data for $H_2O(g)$. The β values for SmO, other monoxides, and all gaseous oxides of the LRTE were calculated from detailed consideration of the gas phase equilibria using the method described by Fegley and Palme [5]. The f values for $SmO_{1.5}(s)$ and all LRTE solid oxides were calculated from mass balance constraints (i.e., the sum of fractions of all oxides of a given element = 1) and the activities of the pure oxides at the particular temperature, pressure, and oxygen fugacity. Because gas phase and gas-solid equilibrium calculations are coupled, the two sets of calculations were performed simultaneously using iterative techniques. As an internal check on the calculations, all possible

paths for condensation of a single oxide were calculated, for example:

$$Ce(g) + \tfrac{3}{2}H_2O(g) = CeO_{1.5}(s) + \tfrac{3}{2}H_2(g) \quad (9)$$

$$CeO(g) + \tfrac{1}{2}H_2O(g) = CeO_{1.5}(s) + \tfrac{1}{2}H_2(g) \quad (10)$$

$$CeO_2(g) + \tfrac{1}{2}H_2(g) = CeO_{1.5}(s) + \tfrac{1}{2}H_2O(g) \quad (11)$$

These internal checks always gave identical results, indicating that no errors were present in the METKON code and that the thermodynamic data set was internally consistent.

3. 50% oxide condensation temperatures

The calculated 50% oxide condensation temperatures for the 26 LRTE included in the calculations are shown in Table 2. The temperatures are for the ideal solid solution in perovskite baseline model, and are tabulated at 10^{-3}, 10^{-6}, and 10^{-9} bars total pressure for comparison with the calculated 50% condensation temperatures of refractory siderophiles at these pressures in Fegley and Palme [5].

The most refractory oxides at all pressures considered are ZrO_2, HfO_2, Sc_2O_3, and Y_2O_3, which also are the only oxides to consistently condense as pure phases before perovskite forms at 1676 K (10^{-3} bars), 1463 K (10^{-6} bars), or 1296 K (10^{-9} bars). At 10^{-9} bars total pressure, Lu_2O_3 and Er_2O_3 also condense as pure phases a few degrees above the perovskite condensation temperature. However, the small temperature difference is probably not significant because it lies within the ΔT range corresponding to uncertainties in the thermodynamic data for the LRTE oxides and perovskite.

Lu_2O_3, Er_2O_3, ThO_2, Ho_2O_3, Tb_2O_3, Tm_2O_3, and Dy_2O_3 are so refractory that they are $> 50\%$ condensed in ideal solid solution in perovskite within 1 K of perovskite condensation. Gd_2O_3 is only slightly less refractory. The light-REE oxides Nd_2O_3, Pr_2O_3, Sm_2O_3, and La_2O_3 have similar volatilities, while Yb_2O_3, Ce_2O_3, and Eu_2O_3 are much more volatile. The stable dioxide gas CeO_2 [23] is responsible for the calculated relative volatility of Ce. Other REE dioxide gases (e.g., LaO_2; NdO_2; GdO_2; HoO_2) were not included in our final calculations because Fegley [33] showed that the published thermodynamic data for these gases disagree with measured vapor pressure data for solid REE oxides, and hence probably are incorrect. We did include LaO_2, NdO_2, GdO_2, and HoO_2 in an earlier set of calculations, and we are satisfied that the thermodynamic data are incorrect because the calculated volatility of these REE totally disagrees with their abundances in Allende CAI's. Eu_2O_3 is much more volatile than Yb_2O_3 if

TABLE 2

Calculated 50% oxide condensation temperatures (K) for ideal solid solution in perovskite

Oxide	Total pressure (bars)		
	10^{-3}	10^{-6}	10^{-9}
ZrO_2 [a]	1786	1594	1437
HfO_2 [a]	1753	1577	1434
Sc_2O_3 [a]	1724	1524	1366
Y_2O_3 [a]	1692	1499	1346
Lu_2O_3	1676	1463	1302
Er_2O_3	1676	1463	1303
ThO_2	1676	1463	1296
Ho_2O_3	1676	1463	1296 [b]
Tb_2O_3	1676	1463	1296
Tm_2O_3	1676	1463	1296
Dy_2O_3	1675	1463	1296
Gd_2O_3	1674	1462	1296
UO_2	1663	1437	1253
PuO_2 / Pu_2O_3	1654 [c]	1445 [c]	1280 [c]
Nd_2O_3	1640	1430	1260
Pr_2O_3	1636	1420	1254
Sm_2O_3	1633	1433	1275
La_2O_3	1621	1410	1247
Ta_2O_5	1614	1418	1265
NbO / NbO_2	1609 [c]	1362 [c]	1190 [c]
Yb_2O_3	1549	1392	1263
VO / V_2O_3	1542 [c]	1308 [c]	1122 [c]
Ce_2O_3	1532	1286	1109
Eu_2O_3	1398 [d,e]	1232 [d]	1104 [d]
SrO	1275 [d,f]	1116 [d]	992 [d]
BaO	1227 [d,f]	1052 [d]	919 [d]

[a] Oxide condenses as a pure phase before perovskite condenses at all pressures considered.

[b] Ho_2O_3 is more refractory than ThO_2 at $p = 10^{-9}$ bars pressure.

[c] 50% condensation temperature calculated by adding the amounts of both oxides condensed (see text).

[d] Calculated assuming perovskite is still present as a host phase (see text).

[e] 50% condensation temperature of Eu_2O_3 in melilite (assuming ideal solid solution) is 1488 K.

[f] 50% condensation temperatures of SrO and BaO in melilite (assuming ideal solid solution) are 1375 K and 1324 K, respectively (see text).

ideal solid solution in perovskite is considered. However, the calculated Eu_2O_3 50% condensation temperature (1398 K at 10^{-3} bars) is lower than the temperature (1409 K) at which perovskite disappears under equilibrium conditions [34]. It also is significantly lower than the condensation temperature ($\sim$ 1430 K) of the bulk of the condensible matter in the solar system in the form of olivine and Fe-metal [5,34]. Thus, if Eu condensed in ideal solid solution in perovskite, CAI's should not contain a significant amount of Eu unless they also contained large amounts of olivine and Fe-metal. Grossman et al. [14] concluded that most Eu condensed in solid solution in melilite, and our calculations show that at 10^{-3} bars the 50% condensation temperature of Eu_2O_3 in melilite (assuming ideal solid solution) is 1488 K, which is within the calculated stability field of melilite [34].

The calculated 50% condensation temperatures for the other LRTE also display interesting trends. U and Pu have similar relative volatilities (intermediate between those of Gd and Nd). UO_2 is the only important solid U-oxide at the canonical nebular oxygen fugacity, but Pu_2O_3 and PuO_2 are of approximately equal importance. Pu_2O_3 is slightly more refractory than PuO_2 at the canonical nebular oxygen fugacity; their respective 50% condensation temperatures are 1634 K and 1620 K. Similar situations also hold for Nb and V, elements for which two different oxidation states are important at the canonical nebular oxygen fugacity. The computed 50% condensation temperatures for the element pairs Nb-Ta and V-Yb are very similar, but the measured abundances of the elements in each pair are noticeably different in several types of Allende CAI's (discussed in section 4.2).

Finally, SrO and BaO are the two most volatile LRTE oxides included in our calculations: their respective 50% condensation temperatures for ideal solid solution in perovskite are 1275 K and 1227 K at 10^{-3} bars. However, Sr apparently occurs in melilite in coarse-grained Allende CAI's while Ba occurs in a different phase than Sr or most other LRTE [14]. The 50% condensation temperatures for SrO and BaO ideal solid solution in melilite are 1375 K and 1324 K, respectively. But these temperatures are lower than the calculated temperature (1438 K) at which melilite disappears [34].

Tanaka and Okamura [35] and El Goresy et al. [36] observed Ba-rich phases in fine-grained Allende CAI's and in an Essebi CAI, respectively; Tanaka and Okamura [35] identified the Ba-rich phase they observed as $BaTiO_3$, but it has not been reported by other groups. Neither $SrTiO_3$ nor $BaTiO_3$ are stable as pure phases in the solar nebula unless their activity coefficients for ideal solid solution in perovskite are significantly larger than 1. Fegley [37] concluded from a thermodynamic analysis of the relevant phase diagrams that although the $SrTiO_3$-$CaTiO_3$ system is close to ideality, activity coefficients of 10–20 are implied for $BaTiO_3$-$CaTiO_3$ solid solutions. His calculated 50% condensation temperatures for $SrTiO_3$ ideal solid solution in perovskite and $BaTiO_3$ non-ideal solid solution ($\gamma = 10$) at 5×10^{-3} bars are 1602 K and 1500 K, respectively. If we adopt his values, Sr would be as volatile as Nb or Ta, and Ba would be slightly more volatile than Ce. However, because of the large difference between the 50% condensation temperatures for Sr and Ba as oxides in perovskite or as titanates and the possibility that Sr and Ba condense as melilite analogs or aluminates (such as $SrAl_{12}O_{19}$ or $BaAl_{12}O_{19}$) for which no reliable thermodynamic data are available, we do not recommend specific values for their condensation temperatures.

3.1. Some effects of non-ideal solid solution

Despite a decade of debate, the effect of non-ideal solid solution on LRTE abundances in Allende CAI's remains uncertain because activity coefficients are not available for the relevant solid solutions. However, calculations for selected LRTE that are based on qualitative assumptions are interesting because they illustrate the relative impor-

TABLE 3

Effect of activity coefficients (γ) on SrO and BaO 50% condensation temperatures (K)

Sr		Ba	
γ	T	γ	T
1.0	1375	1	1324
0.2	1428	2	1301
0.1	1453	5	1272
0.05	1478	10	1251
0.01	1535	25	1224

TABLE 4

Effect of activity coefficients (γ) on actinide 50% condensation temperatures (K)

γ^{4+}	Th	U	Pu
1	1676.0	1663	1654
50	1675.4	1546	1634.5
100	1674.8	1526	1633.5
500	1670	1481	1633.5
1000	1663	1460	1633.5
5000	1630	1427	1633.5
10,000	1609	1412	1633.5

tance of crystal-chemical and volatility effects during the condensation of LRTE.

The 50% condensation temperatures for different SrO and BaO non-ideal solid solutions in melilite are shown in Table 3. Table 4 presents analogous calculations for Th, U, and Pu, which have very similar tetravalent ionic radii of 1.12 Å, 1.08 Å, and 1.06 Å, respectively (in VIII coordination). Very large changes in the assumed activity coefficient for Pu^{4+} have only a small effect on the Pu 50% condensation temperature because Pu_2O_3 also is refractory; the refractory nature of ThO_2 similarly counterbalances very large ($10^4\times$) increases in the Th^{4+} activity coefficient. But because UO_2 is more volatile than Pu or Th and no other valence states of U are important at the canonical nebular oxygen fugacity, the 50% condensation temperature of UO_2 decreases substantially as the assumed activity coefficient of U^{4+} is increased.

4. Refractory trace-element abundances

4.1. Lithophile refractory trace elements

Mean LRTE abundances in Group I,V Allende CAI's and in Ca-rich and Ca-poor varieties of Group II and Group III Allende CAI's are shown in Fig. 1 and Table 5. The LRTE are listed in order of increasing volatility in Fig. 1, using the criteria and reasoning discussed below.

Super-refractory LRTE. We classify Zr, Hf, Y, and Sc as super-refractory lithophile trace elements because our calculations indicate they condense as pure oxides before perovskite condenses (Table 2), and because they generally are greatly enriched in most ultra-refractory inclusions (i.e., CAI's with REE patterns complementary to those in Group II inclusions). We believe that the relative enrichments of super-refractory lithophiles in ultra-refractory inclusions can be used to determine their relative volatility. Hf is $>20\times$ more enriched than Sc in the Ornans ultra-refractory inclusion RNZ [39], Hf and Zr each are $>5\times$ more enriched than Sc in the Murchison ultra-refractory inclusion SH-2 [20], and Hf is $\sim 1.2\times$ more enriched than Zr in SH-2 [20]. These abundance data indicate that Sc is the most volatile super-refractory lithophile, even though Sc is $>3\times$ more

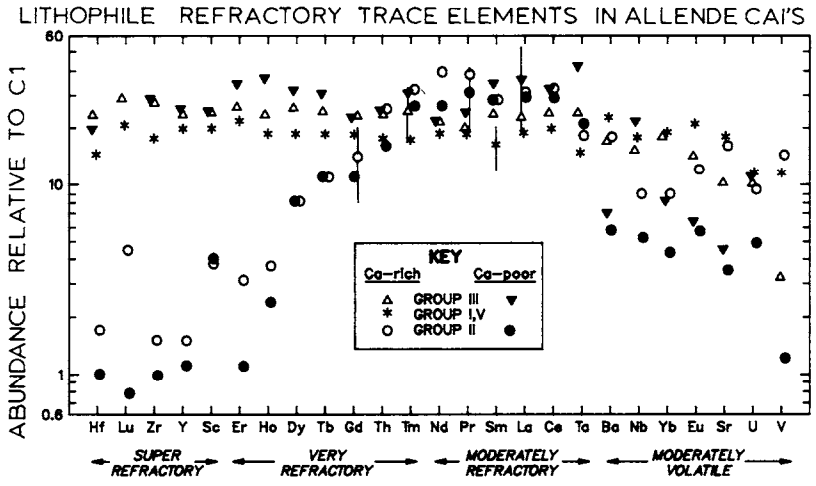

Fig. 1. Mean LRTE abundances in Allende CAI's. Error bars show average $\pm 1\sigma$ standard deviations around the mean for the composite data (not individual analyses) for each type of inclusion. Data compiled from [1,6–18] and H. Palme (unpublished); C1 abundance data in Anders and Ebihara [38] were used for the normalizations.

TABLE 5

Average refractory trace-element abundances in Allende CAI's (ppm) (1σ standard deviations shown in parentheses) [a]

	Group I,V		Group III				Group II			
			Ca-rich		Ca-poor		Ca-rich		Ca-poor	
Lanthanides										
La	4.2	(0.72)	5.5	(1.3)	8.4	(3.9)	7.2	(4.5)	6.9	(2.3)
Ce	12	(1.8)	15	(6.0)	20	(13)	20	(11)	18	(4.8)
Pr	1.7	(0.23)	1.9	(0.4)	2.2	(–)	3.5	(1.8)	2.9	(1.1)
Nd	8.0	(1.6)	10	(3.7)	10	(–)	18	(9.9)	12	(4.3)
Sm	2.4	(0.54)	3.6	(0.89)	5.0	(3.3)	4.1	(2.1)	4.2	(1.3)
Eu	1.1	(0.18)	0.76	(0.30)	0.36	(0.11)	0.65	(0.25)	0.31	(0.12)
Gd	3.5	(0.60)	4.8	(1.2)	4.6	(–)	2.8	(1.2)	2.2	(1.2)
Tb	0.63	(0.16)	0.89	(0.19)	1.1	(0.42)	0.40	(0.15)	0.39	(0.22)
Dy	4.5	(0.86)	6.4	(1.6)	7.8	(2.3)	2.0	(0.82)	2.0	(1.1)
Ho	1.0	(0.19)	1.3	(0.35)	2.0	(–)	0.20	(0.05)	0.13	(0.07)
Er	3.3	(0.67)	4.2	(1.0)	5.4	(–)	0.50	(0.33)	0.17	(0.04)
Tm	0.43	(0.09)	0.61	(0.20)	0.76	(–)	0.79	(0.28)	0.63	(0.22)
Yb	2.8	(0.61)	2.9	(1.3)	1.3	(–)	1.4	(0.36)	0.68	(0.27)
Lu	0.48	(0.08)	0.72	(0.14)	–	(–)	0.11	(0.04)	0.019	(0.009)
Actinides										
Th	0.50	(0.10)	0.70	(0.38)	0.71	(–)	0.72	(0.16)	0.45	(0.26)
U	0.090	(0.029)	0.080	(0.034)	0.09	(–)	0.076	(0.049)	0.040	(0.015)
Transition metals										
Sc	107	(20)	142	(31)	143	(–)	22	(11)	23	(8.7)
V	637	(103)	180	(–)	–	(–)	802	(–)	66	(29)
Y	28	(7.9)	36	(11)	38	(–)	2.3	(1.2)	1.6	(0.76)
Zr	63	(20)	101	(13)	106	(–)	5.5	(3.0)	3.6	(1.8)
Nb	4.3	(1.4)	3.7	(1.7)	5.5	(–)	2.2	(–)	1.3	(0.52)
Hf	1.7	(0.60)	2.9	(0.84)	2.4	(–)	0.20	(0.08)	0.12	(–)
Ta	0.24	(0.09)	0.41	(0.08)	0.72	(–)	0.30	(–)	0.36	(0.10)
Alkaline earths										
Sr	134	(31)	80	(34)	36	(–)	125	(49)	28	(13)
Ba	49	(13)	38	(14)	16	(–)	41	(16)	13	(4.7)
Refractory metals										
Ru	8.9	(2.5)	17	(5.9)	–	(–)	1.2	(0.63)	1.4	(0.18)
Rh	1.2	(0.41)	1.3	(0.54)	–	(–)	0.15	(–)	0.28	(–)
Re	0.56	(0.15)	1.0	(0.37)	–	(–)	0.013	(0.007)	–	(–)
Os	7.2	(2.2)	12	(3.9)	–	(–)	0.25	(0.02)	0.50	(0.16)
Ir	7.5	(2.1)	14	(4.5)	–	(–)	0.30	(0.09)	0.45	(0.22)
Pt	10	(1.8)	15	(6.3)	–	(–)	0.62	(–)	0.74	(0.20)

[a] Excluding the anomalous trace-element abundances discussed in Appendix 1.

enriched than Zr or Y in the Ornans ultra-refractory inclusion OSCAR [40]. We believe that the very large Sc enrichment in OSCAR is due to the crystal-chemical affinity of Sc for clinopyroxene (discussed in section 5.1). We also classify the heavy-REE Lu as super-refractory because Lu and Hf are equally enriched in RNZ [39], and Lu is $> 3\times$ more enriched than Sc or any other heavy REE in SH-2 [20].

Very refractory LRTE. The 50% oxide condensation temperatures of Th and the heavy REE Gd, Tb, Dy, Ho, Er, and Tm are only a few K less than the condensation temperature of perovskite (Table 2). We have used the relative enrichments of these very refractory lithophiles in ultra-refractory inclusions to modify our calculated volatility sequence for them. The heavy REE and Th abundances in RNZ [39] and SH-2 [20] suggest that the

relative volatility of six of the very refractory LRTE is Er < Ho < Tm ~ Dy < Tb < Th. But studies of Group II inclusions indicate that Tm probably is the most volatile trace element in this group [4,21] and our condensation calculations in Table 2 indicate that Gd is more volatile than Dy or Tb.

Moderately refractory LRTE. The light REE La, Pr, Nd, and Sm, the actinides U and Pu, and the transition metals Nb and Ta have 50% oxide condensation temperatures greater than 1600 K at $p = 10^{-3}$ bars (Table 2); these eight trace elements largely condense in the temperature range in which hibonite, perovskite, and melilite (the important LRTE hosts in CAI's) form or disappear by various reactions. We have adopted the calculated volatility sequence for the moderately refractory LRTE in Table 2, except for the following changes: (1) because Ce is approximately as enriched as the other moderately refractory light REE in SH-2 [20] and Group II inclusions (Fig. 1), we assign it a volatility slightly less than that of La; and (2) Nb and U are significantly less enriched than the moderately refractory light REE in Group II and Group III Allende CAI's (Fig. 1), indicating that they are less refractory than these lanthanides (see section 4.2).

Moderately volatile LRTE. The lanthanides Yb and Eu, the transition metal V, and the alkaline-earths Sr and Ba have the lowest oxide condensation temperatures of the 26 LRTE we considered. We classify them as moderately volatile LRTE, and add Nb and U to this group for the reason discussed in the previous section. We have determined the relative volatility of these seven trace elements by also considering their abundances in Allende CAI's (Fig. 1). U and V are significantly less enriched than the other moderately volatile LRTE in Group I,V Allende CAI's (which are relatively unfractionated), indicating that they are the most volatile trace elements in this group. We have adopted the relative volatility sequence for Nb, Yb, Eu, and Sr in Table 2, and infer that Ba is the most refractory member of this group because Ba is more enriched than the other moderately volatile LRTE in Group I,V Allende CAI's.

4.2. LRTE abundances

Except for Hf (which we discuss in section 5.5) and Ta, LRTE more refractory than U are approximately uniformly enriched to ~ 16–20 × chondritic levels in Group I,V Allende CAI's. LRTE more refractory than Ba are approximately uniformly enriched to ~ 24–36 × chondritic levels in Group III CAI's. Thus, Group I,V CAI's represent on average ~ 5–6 wt.% of condensible cosmic material while Group III CAI's represent on average only ~ 3–4 wt.% of condensible cosmic material.

The moderately refractory light REE are approximately unformly enriched to ~ 30–40 × chondritic levels in Group II Allende inclusions: for these trace elements, Group II CAI's on average are slightly more refractory than Ca-rich Group III CAI's, and represent ~ 2.5–3 wt.% of condensible cosmic material. The abundances of more refractory LRTE in Group II inclusions decrease systematically in parallel with increases in their respective oxide condensation temperatures (except for U, Tm, Th, and Sc). The generally smooth fractionation pattern among the super- and very refractory LRTE in Group II inclusions shows that the empirical modifications we made to the calculated volatility sequence (which generally were based on their abundances in ultra-refractory inclusions) are valid. The super-refractory lithophiles Hf, Zr, and Y are depleted to only approximately chondritic levels in spinel-rich Group II CAI's and to ~ 1.5 × chondritic levels in Ca-rich Group II CAI's.

Among the moderately volatile LRTE, the large depletion of V in spinel-rich Group II inclusions to approximately chondritic levels is puzzling (especially since V is not greatly depleted in Ca-rich Group II inclusions). Spinel is a very favorable host for V: in seven of eight spinel-rich Group II inclusions we have studied, spinels contain ~ 0.15–0.65 wt.% V_2O_3 (i.e., ~ 1000–4400 ppm V) [41]. The spinel-rich Group II inclusions we analyzed only need to contain ~ 6–30 wt.% spinel for V to be enriched in them to 5 × chondritic levels (the level to which the other relatively volatile LRTE typically are enriched in this type of CAI). Since all of the spinel-rich Group II inclusions we studied contain > 25 vol.% spinel, we conclude that V is enriched to ⩾ 5 × chondritic levels in them except for one of our inclusions

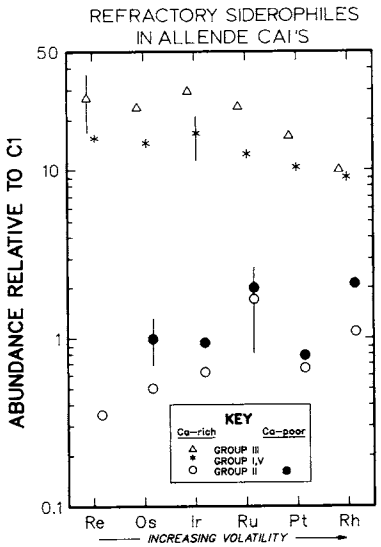

Fig. 2. Mean refractory siderophile abundances in Allende CAI's (error bar symbols as in Fig. 1). Refractory siderophile abundances in spinel-rich Group II inclusions are based on data from only five inclusions (see text). Data compiled from [1,8–11,14–18] and H. Palme (unpublished); C1 abundance data in Anders and Ebihara [38] were used for the normalizations.

(0702, which contains V-poor spinel). The V anomaly in Fig. 1 could simply be an artifact of the small number (i.e., three) of analyses reported by Conard [10] and H. Palme (unpublished); but V also is relatively depleted in a spinel-rich Group II Efremovka inclusion [42].

4.3. Refractory siderophile abundances

Mean enrichment factors of refractory siderophiles in the various types of Allende CAI's are shown in Fig. 2. The refractory siderophiles are listed in order of increasing volatility, on the basis of the alloy condensation temperatures in Fegley and Palme [5]. We excluded W and Mo from our compilation because these refractory siderophiles commonly were depleted from CAI's by high-temperature oxidation processes [5].

In Group I, III, and V CAI's the relative abundance of refractory siderophiles systematically decreases from Ir → Rh (in parallel with their respective condensation temperatures) [16]. Ir is slightly more enriched in these inclusions than Re and Os (which are more refractory); we cannot explain this apparent anomaly. Refractory siderophile abundances show that Group III CAI's are more refractory than group I,V CAI's: the very refractory siderophiles Re → Ru are approximately twice as enriched in Group III CAI's (to ~ 24–30 × chondritic levels) than they are in Group I,V CAI's (to only ~ 12–16 × chondritic levels). Another parameter that shows that Group III CAI's are more refractory than Group I,V CAI's is the degree of fractionation among the refractory siderophiles on the basis of their relative volatility (which is expressed by the steepness of the slopes of the lines connecting the data for Ir → Rh in Fig. 2). For example, the mean C1-normalized Ir/Rh ratio in Group III CAI's is 3.1, while this ratio is only 1.7 in Group I,V CAI's. Except for the anomalous Ca-rich Group II CAI's A-19 and EK 1-4-1 (discussed in section 5.1), Ca-rich and spinel-rich Group II Allende inclusions contain $\leqslant 2\times$ chondritic levels of refractory siderophiles.

4.4. The relative volatility of refractory siderophile and refractory lithophile trace elements

The 50% condensation temperatures of refractory metal alloys in Fegley and Palme [5] and of LRTE oxides in Table 2 can be used to compare the relative volatility of these two groups of trace elements. Re and Os are much more refractory than any LRTE since at $p = 10^{-3}$ bars the 50% condensation temperatures of Re and Os each are ~ 100–150 K higher than the 50% condensation temperatures of the LRTE with the highest condensation temperatures (Hf and Zr). Trace-element abundances in ultra-refractory inclusions support this conclusion: Re and Os each are more enriched than any LRTE in RNZ, SH-2, and ES-1 [20,36,39]. The 50% condensation temperature of Ir (1683 K) suggests that Ir is less refractory than the super-refractory lithophiles but more refractory than the very refractory LRTE. However, Ir is approximately as enriched as the most enriched LRTE in SH-2 [20] and ES-1 [36], and Ir is much more enriched than any LRTE in RNZ [39]. This indicates that Ir is more refractory than condensation calculations would suggest.

5. Discussion

Allende CAI's initially were interpreted to be aggregates of refractory crystalline condensates

that formed in the solar nebula [8], but more recently it has been recognized that many Ca-rich CAI's were once at least partially molten [43]. The relative importance of condensation vs. distillation processes in the primitive solar nebula remains controversial; one interpretation is that igneous Ca-rich CAI's formed during the evaporation and melting of interstellar dust aggregates [44], and that spinel-rich inclusions contain fractionated residues of primitive dust aggregates that lost Ca-rich partial melts during distillation [32,45,46]. In this section, we elect to discuss the origin of Allende CAI's and refractory trace-element abundance patterns generally (but not exclusively) using the distillation and partial melting model that we prefer.

5.1. Group II inclusions

Davis and Grossman [21] concluded that the REE, Zr, and Ir occur in Group II Allende inclusions in two different components, in one of which they are equally enriched to ~ 0.1–$5.4\times$ chondritic levels. The two most refractory REE (Lu and Er) occur at approximately chondritic levels in spinel-rich Group II CAI's (Fig. 1). Because most other super-refractory lithophile trace elements (i.e., Zr; Hf; Y) also occur at approximately chondritic levels in these inclusions, we infer that a "chondritic component" is the carrier for the low concentrations of all super-refractory lithophiles (excluding Sc) in spinel-rich Group II inclusions. Furthermore, it is not unreasonable to infer that this component contains the other LRTE at approximately chondritic levels as well.

The super-refractory trace-element depletions in Group II inclusions have been explained by the physical fractionation of very refractory host phases, such as perovskite [4,21] or hibonite [20] at very high temperatures only a few hundreths of a degree below their condensation temperatures, or of oxide-rich Fremdlinge at relatively low temperatures [2]. Sc is significantly less depleted in Group II inclusions than are other LRTE with comparably-high oxide condensation temperatures (e.g., Zr; Hf; Y) (Fig. 1). Sc seems to have an affinity for a greater variety of CAI carriers than do the other super-refractory lithophiles, which typically are concentrated in perovskite [47]: e.g., El Goresy et al. [36] analyzed Sc-rich Ti-Al-pyroxenes (containing as much as 6.2 wt.% Sc_2O_3) in an Essebi CAI, and the Sc/Hf ratio in a hibonite-rich separate from the Group I CAI CG-II is $\sim 2\times$ the ratio in the bulk inclusion [15]. Perovskite apparently is a less favorable host for Sc than for several other super-refractory lithophile trace elements [48]; Allen et al. [49] showed that perovskites in CG-11 have a mean C1-normalized Sc/Zr ratio of only ~ 0.3.

The super-refractory carrier that was fractionated probably was a minor phase whose loss did not significantly change the bulk composition of the reservoir(s) from which all mineralogical varieties of Allende inclusions subsequently formed by various processes [32], since Group II REE patterns occur in all mineralogical varieties of Allende CAI's (i.e., Type A, B, and C CAI's and spinel-rich inclusions) and in some olivine-rich inclusions as well [47]. We suggest that only a *single* minor carrier was fractionated as discrete grains to produce Group II super-refractory lithophile depletions, and that relatively less Sc was lost from the reservoir(s) in which Group II inclusions later formed because at the time of the fractionation a significant proportion of Sc was present in each of several carriers (e.g., perovskite; hibonite; Ti-Al-pyroxene), some of which were not fractionated. In section 5.2 we show why it is unlikely that the super-refractory lithophile carrier was hibonite (or was enclosed by this mineral) at the time of the Group II fractionation.

Although most Group Allende inclusions are depleted in refractory siderophiles and the most refractory LRTE, this does not *require* that the Group II fractionation occurred at high temperatures in the solar nebula (i.e., before the more volatile LRTE condensed). We have postulated that oxide-rich Fremdlinge were the refractory siderophile and super-refractory lithophile carrier, and that these Fremdlinge were physically fractionated at low temperatures before Group II inclusions subsequently formed by distillation [2]. Although Grossman et al. [50] recently showed that a large sulfide-rich, oxide-poor Allende Fremdling contains low concentrations of Sc, Palme et al. [39] and Lavrukhina et al. [51] have analyzed oxide-rich Fremdlinge from Ornans and Kainsaz that do contain high concentrations of Sc. The abundance of at least one refractory siderophile has been measured in 30 Group II Allende inclusions; in 28 of these inclusions, refractory

siderophiles are at least as depleted as are the super-refractory LRTE. Thus, if oxide-bearing Fremdlinge generally are enriched in super-refractory LRTE, our proposal that Group II inclusions distilled from Frendlinge-poor dust explains the correlation between refractory siderophile and super-refractory LRTE depletions that are observed in $>90\%$ of Group II Allende inclusions, and why (in most cases) refractory siderophiles are more depleted than are super-refractory LRTE in these objects.

Refractory siderophile fractionations in Group II Allende inclusions generally mimic (but are less extreme than) the very large fractionations seen between super-refractory, very refractory, and moderately refractory LRTE in these inclusions [52]. Refractory metal concentrations in the ultra-refractory inclusions RNZ [39], SH-2 [20], and ES-1 [36] confirm condensation calculations by Fegley and Palme [5] which show that Re and Os are much more refractory than Ru, which in turn is much more refractory than Pt and Rh. In addition, the enrichment of Ru in each of these ultra-refractory CAI's is intermediate between the enrichments of various heavy REE, confirming calculations by Fegley and Palme [5] that Ru is approximately as volatile as these very refractory LRTE. In Group II Allende inclusions, the relative abundance of refractory siderophiles generally increases from Re to Ru, then decreases for Pt before increasing again for Rh (Fig. 2). This pattern parallels the REE fractionation pattern found in Group II Allende inclusions, including an unexplained positive anomaly for the most volatile trace-element in each respective group (Eu and Rh, respectively) [53]. We doubt if the refractory siderophile fractionation patterns in Fig. 2 simply are artifacts of the contamination of extremely refractory metal-poor Group II inclusions by chondritic-composition material (e.g., meteorite matrix): mass-balance constraints would require an unreasonably large amount of contamination (>50 wt.%) for Group II inclusions to consequently contain ~ 0.6–$2\times$ chondritic abundances of refractory siderophiles.

Two Ca-rich Group II Allende inclusions (EK-1-4-1; A-19) discussed in Appendix 1 contain relatively high concentrations of refractory siderophiles; Ekambaram et al. [20] described a spinel-rich Group II Murchison inclusion (SH-4) that also contains high concentrations of refractory siderophiles. These three refractory metal-rich Group II inclusions have small positive Eu and Yb anomalies as well (rather than the large negative Eu and Yb anomalies that typically occur in Group II inclusions). But in A-2 [10] and FG-16 [12], the other two Group II Allende inclusions that also have small positive Eu and Yb anomalies, the refractory siderophiles are not anomalously enriched. Thus, there is no simple relationship among anomalous refractory siderophile, Eu, and Yb enrichments in Group II Allende inclusions.

Th and Tm (like Sc) are much more enriched in Group II inclusions than would be anticipated by their position in our calculated condensation sequence (Table 2), and U is much less enriched than other LRTE of similar volatility (i.e., the light REE, excluding Eu) (Fig. 1). The Tm anomaly has long been recognized [6] and defies easy explanation (requiring unreasonably large changes in the activity coefficients of the heavy REE in perovskite) [4,21]. On the basis of Th and REE abundances in Group II CAI's, Boynton [54] suggested that the relative volatilities of Th and Gd are approximately equal. The more comprehensive data in Fig. 1 indicate that Th is slightly more abundant than Gd in Ca-poor Group II inclusions, and that Sm and Th abundances are nearly equal in Ca-rich Group II inclusions. Using Boynton's reasoning, we infer from Tables 2 and 4 that in Ca-poor Group II inclusions a Th^{4+} activity coefficient (γ) of ~ 500 is implied, while in Ca-rich Group II inclusions an activity coefficient of ~ 5000 is implied (assuming ideal solid solution for Gd and Sm, respectively).

If these activity coefficients can be applied to the other actinides (all of which have similar ionic radii), in both cases we would expect Pu to be as volatile as Sm (and have a similar 50% condensation temperature), while U would be much more volatile than any REE except perhaps Eu (which in any case may condense in melilite at higher temperatures). In fact, Fig. 1 shows that there is very little difference between the abundances (and, by inference, the relative volatilities) of U and Yb in Ca-poor or Ca-rich Group II inclusions. The apparent lack of a detailed correlation between predicted and empirically-derived relative volatilities of U and REE could simply

indicate that these LRTE are present in another host phase in addition to perovskite. Alternatively, the use of relative abundances to estimate activity coefficients may be incorrect, and the apparent relative volatility of U may be due to the absence of perovskite grains while U condensed (due to grain transport).

5.2. LRTE condensation in hibonite

The condensation calculations in Table 2 are applicable to the condensation of LRTE oxides in perovskite. But perovskite was not the only suitable LRTE carrier at high temperatures in the solar nebula. Hibonite, which is more refractory than perovskite under nebular conditions [32], is another potential host for the LRTE. We have calculated the condensation behavior of the super-refractory and very refractory LRTE in hibonite (again assuming ideal oxide solid solution) (Table 6). To more clearly illustrate the behavior of trace elements that are almost completely condensed in hibonite, we use gas/solid distribution coefficients (D values) normalized to $D_{Zr} = 1$.

A comparison of Tables 2 and 6 shows several interesting results. Hf is more refractory than Zr if ideal solid solution in hibonite is considered; this may explain why Hf is more enriched than Zr in SH-2 (a hibonite-bearing ultra-refractory inclusion). In general, the relative volatilities of the heavy REE are very similar in perovskite and hibonite (in part because we have assumed ideal solid solution in both cases), and very large changes (10^3–$10^4\times$) in LRTE activity coefficients are required to significantly change their relative volatility. Also, the super-refractory nature of Lu is more evident for ideal solid solution in hibonite.

TABLE 6

Condensation of super-refractory and very refractory LRTE in hibonite (ideal solid solution)

LRTE	D	% condensed
Hf	0.05	100
Zr	≡1.0	100
Lu	2.0	100
Er	6.2	> 99
Th	9.2	> 99
Y	16	> 99
Ho	40	> 99
Sc	49	> 99
Tb	67	> 99
Tm	530	> 99
Dy	580	> 99
Gd	910	> 99

Note: Calculations applicable to the condensation temperature of hibonite at $p = 10^{-3}$ bars (i.e., 1730 K [32]).

Ekambaram et al. [20] discussed hibonite as a candidate for the super-refractory LRTE carrier that was fractionated at high temperatures (just below its condensation temperature) prior to the formation of Group II inclusions, but there are two serious problems with this model [55]. Smooth depletions in heavy REE abundances commonly occur in CAI hibonites [56]. Most of these CAI's are very refractory objects: e.g., the heavy REE-depleted hibonites in BB-5, DJ-2, and MUCH-1 are nonetheless greatly enriched in Y, Zr, and/or Hf [20,57]. Thus, if the heavy REE depletions in these hibonites were established by gas/solid reactions alone, it suggests that these very refractory LRTE had a poor affinity for hibonite during condensation at high temperatures, and this mineral is not likely to have been the carrier of the required heavy REE-enriched component. Furthermore, Sc is significantly more enriched than Zr, Hf, or Y in Group II inclusions and in CAI hibonites. Group II inclusions and CAI hibonites should have *complementary* light REE/heavy REE fractionations and Sc/Zr fractionations if these inclusions formed from a reservoir that had lost hibonite; instead, CAI hibonites and Group II inclusions generally have very similar trace-element fractionations.

The LRTE patterns in CAI hibonites could have been established by crystal/liquid partitioning during melting: e.g., the hibonite/melt partition coefficient of Yb is only 0.10 (in air at $T = 1480°C$), while hibonite/melt partition coefficients of La and Sm are 7.2 and 2.15, respectively (M.J. Drake, unpublished). This explanation for the observed heavy-REE depletions in CAI hibonites seems reasonable, and contradicts the vapor/solid condensation model for the origin of BB-5 and MUCH-1 favored by Bar-Matthews et al. [58] and MacPherson et al. [59].

5.3. LRTE fractionations in spinel-rich inclusions

We have proposed that spinel-rich inclusions are refractory residues that lost Ca-rich partial

melts [32]. Ekambaram et al. [20] criticized our partial melting model, in part because spinel-rich Murchison spherules do not show all of the LRTE fractionations that are expected if they had equilibrated with a Ca-rich melt that later was lost. Of course, this criticism logically also should be leveled against the partial melting model for the origin of spinel-rich Murchison spherules independently proposed by MacPherson et al. [59]. But it is important to remember that this criticism is valid only if LRTE carriers in spinel-rich residues *equilibrated* with Ca-rich melts. Equilibrium crystal/liquid partitioning generally requires periods of days or longer for trace elements: e.g., Nagasawa et al. [48] allowed perovskite, spinel, and melilite to crystallize for 3–9 days to achieve equilibrium partitioning of Sc and REE. Although periods of days or more during which spinel-rich inclusions were partially molten are reasonable in the context of canonical (i.e., slow-cooling) solar nebula models, we never have supported such models of their origin. One of us (A.S.K.) has specifically proposed that spinel-rich Allende inclusions formed very rapidly under non-equilibrium conditions during the aerodynamic drag heating of interstellar dust aggregates [46].

An important factor is the rate at which perovskites in contact with a CAI-composition melt would dissolve in the melt. Unfortunately, the dissolution kinetics of perovskite in anhydrous, silicate melts have never been determined. Watson and Harrison [60] measured the kinetics of zircon dissolution in zircon-undersaturated, anhydrous felsic melts. Assuming that perovskite has similar dissolution kinetics, we estimate that a 5 μm perovskite grain will dissolve in an *undersaturated* silicate melt in ~ 6 minutes at $T = 1400\,^{\circ}C$. But it is uncertain that a CAI melt would be greatly undersaturated with respect to perovskite. Furthermore, perovskite grains in spinel-rich Allende inclusions generally are enclosed in larger spinel crystals. Naturally, perovskites encapsulated in spinels will have even longer lifetimes. We think that most perovskites need not have melted during the formation of spinel-rich inclusions if distillation was rapid; unmelted perovskite grains then could have equilibrated with the melt only by solid-state diffusion that might have been slow relative to the time scale of the melting event.

5.4. Ba, Sr, and Eu abundances: constraints on CAI alteration

Because Wark [61] showed that melilite in Allende CAI's was readily altered to feldspathoids, grossular, wollastonite, and other secondary minerals, it remains uncertain how much melilite the spinel-rich Allende inclusions once contained. We previously have interpreted the low Ca/Al ratios in spinel-rich inclusions as a primary feature, and evidence that they formed after the physical fractionation of Ca-rich phases from Al-rich phases [32]. Alternatively, if Ca was preferentially lost during the metasomatic alteration of melilite, spinel-rich Allende inclusions could have contained significant amounts of melilite (and had Ca/Al ratios that were more nearly solar) prior to their alteration [61].

Ba, Sr, and Eu are significantly less enriched in spinel-rich Group II and Group III Allende CAI's (generally to $< 6\times$ chondritic levels) than they are in Ca-rich varieties of these inclusions (generally to $> 12\times$ chondritic levels) (Fig. 1). Grossman et al. [14] concluded that Sr and Eu occur in solid solution in melilite in Ca-rich Allende CAI's because Ca, Sr, and Eu abundances positively correlate with each other in these inclusions. We believe that the relatively low concentrations of Ba, Sr, and Eu in spinel-rich Allende inclusions are evidence that they always contained much less melilite (and other Ca-rich phases) than did Ca-rich CAI's. Of course, if large amounts of Ca diffused out of Allende CAI's during alteration it is possible that Ba, Sr, and Eu also were mobilized during metasomatism. But these three LRTE principally substitute for Ca in host phases, and the secondary Ca-rich minerals found in spinel-rich inclusions (e.g., anorthite; grossular) are suitable hosts for even larger amounts of these trace elements than presently occur in the inclusions. Thus, there seems to be no a priori reason why Ba, Sr, and Eu would be lost during alteration of melilite.

5.5. Large-ion lithophile abundance anomalies in Group I Allende CAI's

Wark [62] first noted that large-ion, high-valence LRTE are less enriched in Group I Allende CAI's than divalent and trivalent LRTE of equivalent volatility, and that this crystal-chemical effect is more strongly developed in Type A CAI's than in Type B CAI's. Hf and Ta show this effect

most strongly in Group I Allende CAI's (Fig. 1); it also may explain the relatively low abundance of U in these inclusions.

An additional factor that probably explains in part why Hf is ~20% less enriched than other LRTE is that the Hf abundance [38] we used for the C1 normalization is too high. Patchett [63], who simultaneously measured the abundance of REE and Hf in two samples of Orgueil by isotope dilution, concluded that Anders and Ebihara [38] overestimated the solar abundance of Hf by 10%; Patchett [63] further noted that the Hf-Nd isotopic evolution of C1 material agrees with that of the Earth if the Hf abundance is adjusted downward by this amount. If the solar abundance of Hf recommended by Patchett [63] (i.e., 107 ppb) is used, the Hf anomaly in Fig. 1 is reduced by 50%.

6. Conclusions

We have used condensation calculations and the abundance patterns of 31 refractory lithophile and siderophile trace elements in the various types of Allende CAI's to interpret the cosmochemical behavior of these elements and to constrain the conditions under which some types of inclusions formed.

Heavy REE depletions are common in CAI hibonites, indicating that these very refractory LRTE had a poor affinity for this mineral under the conditions in which the inclusions formed. Hence, hibonite is not likely to have been the carrier of the heavy REE component that is missing from Group II inclusions (if the hibonites analyzed are condensates). Sc is significantly less depleted in Group II Allende CAI's than are other LRTE with comparably high oxide condensation temperatures. Since Sc generally is more enriched than Zr, Hf, or Y in CAI hibonites, this is additional evidence that the physical fractionation of a minor phase other than hibonite preceded the formation of Group II inclusions. Refractory siderophile fractionations in Group II Allende inclusions mimic LRTE fractionations: i.e., trace elements of intermediate volatility (e.g., Ru; Dy) are less depleted than trace elements that are more refractory (e.g., Os; Lu) or more volatile (e.g., Pt; Yb).

We previously have suggested that spinel-rich Group II and Group III inclusions formed from primitive dust aggregates that lost Ca-rich partial melts by ablation or evaporation when they were distilled in the solar nebula [32]. We suggest that spinel-rich inclusions do not show all of the igneous LRTE fractionations expected if they had equilibrated with a partial melt that later was lost because melting and crystal/liquid fractionation occurred rapidly under non-equilibrium conditions (e.g, during aerodynamic drag heating [46]). In addition, perovskite (the principal host for many LRTE) generally was encased in spinel crystals that largely were never molten.

Acknowledgements

H. Palme generously shared unpublished data on trace-element concentrations in several Allende CAI's. We thank M.J. Drake for sharing unpublished data on hibonite/melt REE partitioning coefficients, H. Palme and R.E. Cohen for helpful discussions, H. Kruse for assistance in coding METKON, B.G. Ballard and M.J. Ruoff for drafting figures, and Shell Oil Company for providing technical assistance in the preparation of this manuscript. We also acknowledge helpful reviews by H.Y. McSween, Jr. and an anonymous referee, and editorial comments by F. Begemann. B.F. was partially supported by NSF grant ATM-84-01232 and NASA grant NAG 9-108 to MIT; he also acknowledges the hospitality of H. Wänke and H. Palme at the MPI für Chemie, Mainz, F.R.G.

Appendix 1—Anomalous refractory trace-element abundances in Allende CAI's

We excluded from the compilation in Table 5 those trace-element abundances in Allende CAI's that differed by more than three standard deviations (i.e., were outside the 99% confidence limits) from the mean of the remaining CAI trace-element population. Using this statistical criterion, we classified 7.5% of the available trace-element data as anomalous.

One group of anomalous data are most of the REE abundances in the seven inclusions shown in Table A-1, which generally are much higher or much lower than the REE abundances in all other Allende CAI's of the same type. If we included the anomalous REE abundances in 3529-45, A-18, B-32, and FG-16 in the compilation in Table 5, the mean REE abundances in Group I,V CAI's and in Ca-poor Group II CAI's would not change significantly, but the respective standard deviations for each REE simply would increase substantially. Approximately 65% of the trace-element abundance data we identified as anomalous are those shown in Table A-1.

The other type of data we excluded are the anomalous

TABLE A-1

Refractory trace-element abundances in anomalous Allende CAI's (ppm) (data shown in italics are not anomalous)

	Group I,V		Group III		Group II		
	3529-45 [a]	A-18 [b]	Ca-rich	Ca-poor	Ca-rich	Ca-poor	
			3529-46 [c]	7R-44A	CG-5 [d]	B-32 [e]	FG-16
La	6.36	1.62	11.6	44.5	16	15.1	0.72
Ce	–	–	–	85	36.7	37	6.2
Pr	2.59	–	4.30	–	–	6.0	–
Nd	13.9	–	22.0	–	–	29	–
Sm	4.20	1.21	6.37	20.4	9.96	9.1	1.13
Eu	1.53	0.41	1.33	0.386	*0.64*	*0.193*	0.51
Gd	5.63	–	8.10	–	–	8.1	–
Tb	1.03	–	1.58	5.73	1.61	1.23	< 0.09
Dy	7.39	1.8	10.6	–	8.8	4.98	< 0.8
Ho	1.64	–	2.68	–	–	0.33	–
Er	*4.30*	–	7.74	–	–	0.42	–
Tm	0.73	–	1.11	–	–	1.36	–
Yb	4.2	0.83	5.29	0.58	*0.9*	*0.41*	1.79
Lu	–	0.15	–	4.63	*0.135*	*0.014*	–
Sc	–	39	–	481	80.1	51	4.5

[a] Ru (20 ppm), Re (0.94 ppm), and Ir (12.6 ppm) also are anomalously high [16].
[b] Hf (0.84 ppm) also is anomalously low (H. Palme, unpublished).
[c] Th (1.66 ppm) and U (0.13 ppm) also are anomalously high [16].
[d] Zr (13.6 ppm), Hf (0.79 ppm), and Ta (0.74 ppm) also are anomalously high [18].
[e] Ta (0.85 ppm) also is anomalously high [10].

abundances of typically only one or two refractory trace elements in CAI's that otherwise do not have trace-element anomalies. In a few cases, anomalous depletions can be explained by the formation of CAI's under relatively oxidizing conditions. Because the Th/U ratio is an important cosmochemical value, we purposely excluded from our compilation in Table 5 several anomalously high U abundances in CAI's for which Th data were not also reported—otherwise, the mean Th/U ratios we determined would have been artificially low.

For the sake of completeness, we subsequently list all other anomalous trace-element data we excluded that are not shown in Table A-1:

Group I,V CAI's: The high abundances of U (0.187 ppm) in CG-1 [14]; Sc (166 ppm) in I-2 [11]; Hf (3.3 ppm) and Pt (16.2 ppm) in A-4 [1]; Ba (104 ppm) in 3529-26 [6]; Ru (16.2 ppm), Rh (2.54 ppm), and Pt (18.7 ppm) in 3529-21 [16]; and Ir in EK-1-07 (16.2 ppm), 5241 (14.5 ppm), and EK-1-42 (14.7 ppm) [13]. The low abundances of Ce (3.7 ppm) and V (52 ppm) in Cl [10]; Lu (0.235 ppm) in CG-11 [15]; and Sc (38.8 ppm) in CAI #9 [8].

Ca-rich Group III CAI's: The high abundances of U in CG-2 (0.237 ppm) and CG-10 (0.263 ppm) [14], and Sc (275.4 ppm) in CG-2 [9]. The low abundance of Ba (5.0 ppm) in B-30 [10].

Ca-rich Group II CAI's: The high abundances of Sc (105 ppm) and Ir (6 ppm) in EK-1-4-1 [17]; Ru (3.9 ppm), Re (0.14 ppm), Os (2.46 ppm), Ir (2.04 ppm), and Pt (4.8 ppm) in A-19 (H. Palme, unpublished); and the Eu and Yb abundances in A-2 [10], EK-1-4-1 [17], and A-19 (H. Palme, unpublished), which contain on average 1.24 ± 0.15 ppm Eu and 2.7 ± 0.20 ppm Yb. The low abundances of Yb (< 0.02 ppm), Nb (0.13 ppm), and Ba (8.6 ppm) in 3529-40 [16].

Ca-poor Group II CAI's: The high abundances of Ce (46 ppm) in A-13 (H. Palme, unpublished); Er (0.49 ppm) in B-29 [10]; and Eu (0.81 ppm) and Yb (1.34 ppm) in FG-20 [12].

References

1 H. Wänke, H. Baddenhausen, H. Palme and B. Spettel, On the chemistry of the Allende inclusions and their origin as high temperature condensates, Earth Planet. Sci. Lett. 23, 1–7, 1974.
2 B. Fegley, Jr. and A.S. Kornacki, The geochemical behavior of refractory noble metals and lithophile trace elements in refractory inclusions in carbonaceous chondrites, Earth Planet. Sci. Lett. 68, 181–197, 1984.
3 L. Grossman, Refractory inclusions in the Allende meteorite, Annu. Rev. Earth Planet. Sci. 8, 559–608, 1980.
4 W.V. Boynton, Fractionation in the solar nebula: condensation of yttrium and the rare earth elements, Geochim. Cosmochim. Acta 39, 569–584, 1975.
5 B. Fegley, Jr. and H. Palme, Evidence for oxidizing conditions in the solar nebula from Mo and W depletions in refractory inclusions in carbonaceous chondrites, Earth Planet. Sci. Lett. 72, 311–326, 1985.

6 B. Mason and P.M. Martin, Geochemical differences among components of the Allende meteorite, Smithson. Contrib. Earth Sci. 19, 84–95, 1977.

7 T. Tanaka and A. Masuda, Rare-earth elements in matrix, inclusions, and chondrules of the Allende meteorite, Icarus 19, 523–530, 1973.

8 L. Grossman, Refractory trace elements in Ca-Al-rich inclusions in the Allende meteorite, Geochim. Cosmochim. Acta 37, 1119–1140, 1973.

9 L. Grossman and R. Ganapathy, Trace elements in the Allende meteorite, I. Coarse-grained, Ca-rich inclusions, Geochim. Cosmochim. Acta 40, 331–344, 1976.

10 R. Conard, A study of the chemical composition of Ca-Al-rich inclusions from the Allende meteorite, 129 pp., M.S. Thesis, Oregon State University, Corvallis, Oreg., 1976.

11 C.-L. Chou, P.A. Baedecker and J.T. Wasson, Allende inclusions: volatile-element distribution and evidence for incomplete volatilization of pre-solar solids, Geochim. Cosmochim. Acta 40, 85–94, 1976.

12 L. Grossman and R. Ganapathy, Trace elements in the Allende meteorite, II. Fine-grained, Ca-rich inclusions, Geochim. Cosmochim. Acta 40, 967–977, 1976.

13 H. Nagasawa, D.P. Blanchard, J.W. Jacobs, J.C. Brannon, J.A. Philpotts and N. Onuma, Trace element distribution in mineral separates of the Allende inclusions and their genetic implications, Geochim. Cosmochim. Acta 41, 1587–1600, 1977.

14 L. Grossman, R. Ganapathy and A.M. Davis, Trace elements in the Allende meteorite, III. Coarse-grained inclusions revisited, Geochim. Cosmochim. Acta 41, 1647–1664, 1977.

15 A.M. Davis, L. Grossman and J.M. Allen, Major and trace element chemistry of separated fragments from a hibonite-bearing Allende inclusion, Proc. 9th Lunar Planet. Sci. Conf., pp. 1235–1247, 1978.

16 B. Mason and S.R. Taylor, Inclusions in the Allende meteorite, Smithsonian Contrib. Earth Sci. 25, 30 pp., 1982.

17 H. Nagasawa, D.P. Blanchard, H. Schimizu and A. Masuda, Trace element concentrations in the isotopically unique Allende inclusion, EK 1-4-1, Geochim. Cosmochim. Acta 46, 1669–1673, 1982.

18 D.A. Wark, The Allende meteorite: information from Ca-Al-rich inclusions on the formation and early evolution of the solar system, 385 pp., Ph.D. Thesis, University of Melbourne, Parkville, Vic., 1984.

19 A.S. Kornacki and J.A. Wood, Petrography and classification of Ca,Al-rich and olivine-rich inclusions in the Allende CV3 chondrite, Proc. 14th Lunar Planet. Sci. Conf., J. Geophys. Res. 89, B573–B587, 1984.

20 V. Ekambaram, I. Kawabe, T. Tanaka, A.M. Davis and L. Grossman, Chemical compositions of refractory inclusions in the Murchison C2 chondrite, Geochim. Cosmochim. Acta 48, 2089–2105, 1984.

21 A.M. Davis and L. Grossman, Condensation and fractionation of rare earths in the solar nebula, Geochim. Cosmochim. Acta 43, 1611–1632, 1979.

22 E. Murad and D.L. Hildenbrand, Dissociation energies of GdO, HoO, ErO, TmO, and LuO; correlation of results for the lanthanide monoxide series, J. Chem. Phys. 73, 4005–4011, 1980.

23 M.A. Mignanelli, P.E. Potter and M.H. Rand, The phase relationships and thermochemical properties of the cerium-oxygen system, a critical assessment, Comm. Europ. Commun., Rep. EUR 7820, 38 pp., 1982.

24 J. Kordis and K.A. Gingerich, Mass spectrometric observations of some polyatomic gaseous rare earth oxides and their atomization energies, J. Chem. Phys. 66, 483–491, 1977.

25 V.P. Glushko, L.V. Gurvich, G.A. Bergman, I.V. Veitz, V.A. Medvedev, G.A. Khachcurvzov, V.S. Yungman, eds., Thermodynamic Properties of Individual Substances, Parts 1–4, High Temperature Institute, Moscow, 1978–1982.

26 R.J. Ackermann and M.S. Chandrasekharaiah, Systematic thermodynamic properties of actinite metal-oxygen systems at high temperatures, in: Thermodynamics of Nuclear Materials 1974, vol. II, pp. 3–26, International Atomic Energy Agency, Vienna, 1975.

27 K.A. Gschneidner, Jr., N. Kippenhan and O.D. McMasters, Thermochemistry of the Rare Earths, Rare-Earth Inf. Center, Ames, Iowa, Rep. 15-RIC-6, 1973.

28 L.B. Pankratz, Thermodynamic Properties of Elements and Oxides, U.S. Bur. Mines Bull. 672, 1982.

29 V.B. Parker, D.D. Wagman and W.H. Evans, Selected Values of Chemical Thermodynamic Properties, Natl. Bur. Stand. Tech. Note 270-6, 1971.

30 V.A. Levitskii, D.Sh. Tsagareishvili and G.G. Gvelesigni, Enthalpy and specific heat of strontium and barium zirconates at high temperatures, High Temp. 14, 69–72, 1976.

31 R. Odoz and K. Hilpert, Evaporation and standard enthalpy of formation of $BaZrO_3(s)$, Z. Phys. Chem. N.F. 102, 191–201, 1976.

32 A.S. Kornacki and B. Fegley, Jr., Origin of spinel-rich chondrules and inclusions in carbonaceous and ordinary chondrites, Proc. 14th Lunar Planet. Sci. Conf., J. Geophys. Res. 89, B588–B596, 1984.

33 B. Fegley, Jr., A comparison of REE and refractory metal oxidation state indicators for the solar nebula (abstract), in: Lunar and Planetary Science XVII, pp. 220–221, Lunar and Planetary Institute, Houston, Texas, 1986.

34 J.M. Lattimer and L. Grossman, Chemical condensation sequences in supernova ejecta, Moon Planets 19, 169–184, 1978.

35 T. Tanaka and K. Okamura, Ultrafine barium titanate particles in the Allende meteorite, Geochim. J. 11, 137–145, 1977.

36 A. El Goresy, H. Palme, H. Yabuki, K. Nagel, I. Herrwerth and P. Ramdohr, A calcium-aluminium-rich inclusion from the Essebi (CM2) chondrite: evidence for captured spinel-hibonite spherules and for an ultra-refractory rimming sequence, Geochim. Cosmochim. Acta 48, 2283–2298, 1984.

37 B. Fegley, Jr., Condensation of barium, strontium, and zirconium in the primitive solar nebula (abstract), in: Lunar and Planetary Science XI, pp. 279–281, Lunar and Planetary Institute, Houston, Texas, 1980.

38 E. Anders and M. Ebihara, Solar-system abundances of the elements, Geochim. Cosmochim. Acta 46, 2363–2380, 1982.

39 H. Palme, F. Wlotzka, K. Nagel and A. El Goresy, An ultra-refractory inclusion from the Ornans carbonaceous chondrite, Earth Planet. Sci. Lett. 61, 1–11, 1982.

40 A.M. Davis, A scandalously refractory inclusion in Ornans (abstract), Meteoritics 19, 214, 1984.
41 B. Fegley, Jr. and A.S. Kornacki, The origin and mineral chemistry of Group II inclusions in carbonaceous chondrites (abstract), in: Lunar and Planetary Science XV, pp. 262–263, Lunar and Planetary Institute, Houston, Texas, 1984.
42 W.V. Boynton, D.A. Wark and A.A. Ulyanov, Trace elements in Efremovka fine-grained inclusion E14: evidence for high temperature, oxidizing fractionations in the solar nebula (abstract), in: Lunar and Planetary Science XVII, pp. 78–79, Lunar and Planetary Institute, Houston, Texas, 1986.
43 E. Stolper, Crystallization sequences of Ca-Al-rich inclusions from Allende: an experimental study, Geochim. Cosmochim. Acta 46, 2159–2180, 1982.
44 D.A. Wark and J.F. Lovering, The nature and origin of type B1 and B2 Ca-Al-rich inclusions in the Allende meteorite, Geochim. Cosmochim. Acta 46, 2581–2594, 1982.
45 R.E. Cohen, A.S. Kornacki and J.A. Wood, Mineralogy and petrology of chondrules and inclusions in the Mokoia CV3 chondrite, Geochim. Cosmochim. Acta 47, 1739–1757, 1983.
46 A.S. Kornacki and J.A. Wood, Mineral chemistry and origin of spinel-rich inclusions in the Allende CV3 chondrite, Geochim. Cosmochim. Acta 49, 1219–1237, 1985.
47 A.S. Kornacki and J.A. Wood, The identification of Group II inclusions in carbonaceous chondrites by electron probe microanalysis of perovskite, Earth Planet. Sci. Lett. 72, 74–86, 1985.
48 H. Nagasawa, H.D. Schreiber and R.V. Morris, Experimental mineral/liquid partition coefficients of the rare earth elements (REE), Sc and Sr for perovskite, spinel and melilite, Earth Planet. Sci. Lett. 46, 431–437, 1980.
49 J.M. Allen, L. Grossman, A.M. Davis and I.D. Hutcheon, Mineralogy, textures and mode of formation of a hibonite-bearing Allende inclusion, Proc. 9th Lunar Planet. Sci. Conf., pp. 1209–1233, 1978.
50 L. Grossman, A.M. Davis, V. Ekambaram, J.T. Armstrong, I.D. Hutcheon and G.J. Wasserburg, Bulk chemical composition of a Fremdling from an Allende Type B inclusion (abstract), in: Lunar and Planetary Science XVII, pp. 295–296, Lunar and Planetary Institute, Houston, Texas, 1986.
51 A.K. Lavrukhina, A.Yu. Ljul, G.M. Kolesov and P.A. Korovajkov, Refractory metal inclusions in Kainsaz CO chondrite: their detection and elemental composition (abstract), in: Lunar and Planetary Science XVI, pp. 481–482, Lunar and Planetary Institute, Houston, Texas, 1985.
52 A.S. Kornacki, The relative volatility of refractory trace elements in Allende CAI's (abstract), in: Lunar and Planetary Science XVI, pp. 455–456, Lunar and Planetary Institute, Houston, Texas, 1985.
53 A.S. Kornacki and B. Fegley, Jr., Fractionation patterns among siderophile and lithophile refractory trace elements in CAI's: implications for grain transport in the solar nebula (abstract), in: Lunar and Planetary Science XVII, pp. 436–437, Lunar and Planetary Institute, Houston, Texas, 1986.
54 W.V. Boynton, Fractionation in the solar nebula, II. Condensation of Th, U, Pu, and Cm, Earth Planet. Sci. Lett. 40, 63–70, 1978.
55 A.S. Kornacki, Was hibonite the carrier of the super-refractory REE component in the solar nebula? (abstract), in: Lunar and Planetary Science XVII, pp. 434–435, Lunar and Planetary Institute, Houston, Texas, 1986.
56 A.J. Fahey, J.N. Goswami, K.D. McKeegan and E. Zinner, Ion probe and track studies of CM hibonites: ^{26}Al, ^{244}Pu, and REE (abstract), in: Lunar and Planetary Science XVI, pp. 227–228, Lunar and Planetary Institute, Houston, Texas, 1985.
57 R.W. Hinton, A.M. Davis and D.E. Scatena-Wachel, Ion microprobe determination of REE and other trace elements in meteoritic hibonite (abstract), in: Lunar and Planetary Science XVI, pp. 352–353, Lunar and Planetary Institute, Houston, Texas, 1985.
58 M. Bar-Matthews, I.D. Hutcheon, G.J. MacPherson and L. Grossman, A corundum-rich inclusion in the Murchison carbonaceous chondrite, Geochim. Cosmochim. Acta 46, 31–41, 1982.
59 G.J. MacPherson, M. Bar-Matthews, T. Tanaka, E. Olsen and L. Grossman, Refractory inclusions in the Murchison meteorite, Geochim. Cosmochim. Acta 47, 823–839, 1983.
60 E.B. Watson and T.M. Harrison, Zircon saturation revisited: temperature and composition effects in a variety of crustal magma types, Earth Planet. Sci. Lett. 66, 295–304, 1983.
61 D.A. Wark, Alteration and metasomatism of Allende Ca-Al-rich materials (abstract), in: Lunar and Planetary Science XII, pp. 1145–1147, Lunar and Planetary Institute, Houston, Texas, 1981.
62 D.A. Wark, Crystal chemical effects on the bulk compositions of Allende Group I Ca-Al-rich inclusions (abstract), in: Lunar and Planetary Science XIV, pp. 822–823, Lunar and Planetary Institute, Houston, Texas, 1983.
63 J. Patchett, REE and Hf in Orgueil: new isotope dilution data for evaluation of the planetary Hf isotopic growth curve and the ^{176}Lu cosmic clock (abstract), Meteoritics 18, 372–373, 1983.